HAL
open science

# Magnetic and crystal structures of the magnetoelectric pyroxene LiCrSi2O6

Gwilherm Nenert, M. Isobe, Clemens Ritter, Olivier Isnard, A.-N. Vasiliev, Y. Ueda

## To cite this version:

Gwilherm Nenert, M. Isobe, Clemens Ritter, Olivier Isnard, A.-N. Vasiliev, et al.. Magnetic and crystal structures of the magnetoelectric pyroxene LiCrSi2O6. Physical Review B: Condensed Matter and Materials Physics (1998-2015), 2009, 79, pp.064416. 10.1103/PhysRevB.79.064416 . hal-00967503

**HAL Id: hal-00967503**

**https://hal.science/hal-00967503v1**

Submitted on 31 Mar 2014

**HAL** is a multi-disciplinary open access archive for the deposit and dissemination of scientific research documents, whether they are published or not. The documents may come from teaching and research institutions in France or abroad, or from public or private research centers.

L'archive ouverte pluridisciplinaire **HAL**, est destinée au dépôt et à la diffusion de documents scientifiques de niveau recherche, publiés ou non, émanant des établissements d'enseignement et de recherche français ou étrangers, des laboratoires publics ou privés.

# Magnetic and crystal structures of the magnetoelectric pyroxene $LiCrSi_2O_6$

G. Nénert,[1,*] M. Isobe,[2] C. Ritter,[3] O. Isnard,[4] A. N. Vasiliev,[5] and Y. Ueda[2]
[1]*CEA-Grenoble INAC/SPSMS/MDN, 17 rue des martyrs, 38054 Grenoble, Cedex 9, France*
[2]*Institute for Solid State Physics, University of Tokyo, 5-1-5 Kashiwa, Chiba 277-8581, Japan*
[3]*Institut Laue-Langevin, Boîte Postale 156, 38042 Grenoble, Cedex 9, France*
[4]*Institut Néel, CNRS, Université Joseph Fourier, Boîte Postale 166, 38042 Grenoble, France*
[5]*Low Temperature Physics Department, Moscow State University, Moscow 119991, Russia*
(Received 6 October 2008; revised manuscript received 29 January 2009; published 24 February 2009)

We investigated the magnetic and crystal structures of the recent reported magnetoelectric system $LiCrSi_2O_6$ by powder neutron diffraction. Below $T_N=11.5$ K, an antiferromagnetic order appears. It is characterized by an antiferromagnetic coupling within the $CrO_6$ octahedra chains and a ferromagnetic coupling between the chains. The magnetic order is commensurate with the lattice with $\mathbf{k}=\mathbf{0}$. The associated magnetic space group is $P2_1'/c$. This symmetry is in agreement with the reported magnetoelectric effect. We show that the magnetic frustration in this system is small. Finally, we discuss our results using a Landau phenomenological model and in the light of the literature.

DOI: 10.1103/PhysRevB.79.064416 PACS number(s): 75.25.+z, 91.60.Pn, 75.50.Ee

## I. INTRODUCTION

In recent years, the coupling between magnetic and dielectric properties in transition-metal oxides gave rise to a significant research effort.[1–3] This effort is governed by the emergence of new fundamental physics and potential technological applications.[2–4] Multiferroic materials exhibit simultaneously (ferro)magnetic, pyroelectric, and ferroelastic properties. Contrary to multiferroic materials, magnetoelectric materials show an induced electrical polarization by a magnetic field. A proper understanding of the interplay between the various physical properties of these two types of materials relies heavily on the knowledge of the detailed crystal and magnetic structures.

Recently pyroxene materials with the general formula $AMSi_2O_6$ ($A$=Li,Na;M=Fe,Cr) have been reported as multiferroic materials.[5] This family of materials provides a large playground for physicists in condensed matter where $A$ may be alkali or alkaline-earth elements, $M$ being various metals with valence state 2+ or 3+ and $Si^{4+}$ can be replaced by $Ge^{4+}$. Due to the presence of chains of octahedra which can be magnetic, this family of materials has attracted much attention. It exhibits interesting properties such as spin gap system in $NaTiSi_2O_6$ (Ref. 6) and low dimensional magnetic system in $LiVGe_2O_6$.[7]

While these pyroxenes have been the subject of various studies,[5–12] the complete magnetic structures are known only for few members of this class.[7,11–13] In order to understand and interpret properly the interplay between the dielectric and magnetic properties of this new multiferroic family, the determination of the magnetic structure of their members is necessary. Jodlauk *et al.*[5] suggested that several members of the pyroxene family among which $LiCrSi_2O_6$ exhibit an incommensurate magnetic structure. This incommensurability of the magnetic structure would be the result of the geometrical magnetic frustration present in this family and would explain the reported multiferroic properties.

In this contribution, we have investigated the crystal and magnetic structures of $LiCrSi_2O_6$ using powder neutron diffraction as function of temperature and magnetic field. We show that $LiCrSi_2O_6$ exhibits a rather unexpectedly simple magnetic structure characterized by $\mathbf{k}=\mathbf{0}$ with a magnetic symmetry compatible with a linear magnetoelectric effect. We discuss this linear magnetoelectric effect using a Landau phenomenological model. Finally we discuss the literature. We illustrate through the known reported magnetic structure of several pyroxenes that all of them exhibit a simple magnetic structure with $\mathbf{k}=0$. In particular, we show that the reported magnetic structure of $LiFeSi_2O_6$ is incompatible with the reported magnetoelectric effect.

## II. EXPERIMENT

Polycrystalline samples of $LiCrSi_2O_6$ were prepared by a solid-state reaction with an appropriate molar ratio of $Li_2CO_3$, $Cr_2O_3$, and $SiO_2$. The weighted mixtures were pressed into pellets and heated at 1273 K in air for several days with one intermediate grinding.

Neutron-diffraction measurements were carried out on powder $LiCrSi_2O_6$. The data were collected with the double-axis multicounter high-flux diffractometer D1B at the Institut Laue-Langevin ILL Grenoble using 2.52 Å wavelength selected by a pyrolytic graphite monochromator. In the configuration used, the resolution of D1B was about full width at half maximum (FWHM) $\sim 0.3°$. The multicounter is composed of 400 cells covering a total angular domain of 80° (in $2\theta$). The data collection was made in the temperature range $1.8<T<15$ K. The stoichiometry of the compound as well as the precise crystal structure was investigated using high-resolution powder data at room temperature, 15 and 1.8 K from D2B diffractometer at the ILL. The measurements were carried out at a wavelength of 1.594 Å corresponding to the (335) Bragg reflexion of a germanium monochromator. The neutron detection is performed with $^3$He counting tubes spaced at 1.25° intervals for D2B. A complete diffraction pattern is obtained after about 25 steps of 0.05° in $2\theta$. D1B and D2B are powder diffractometers operating with the take-off angle of the monochromator at 44° and 135° (in $2\theta$),

 ©2009 The American Physical Society

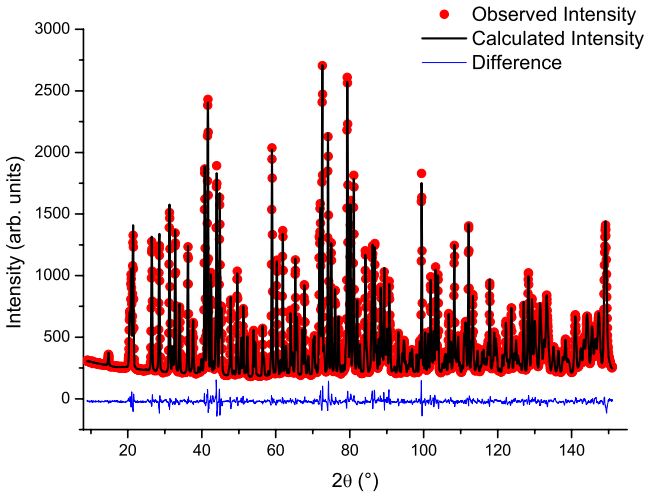


FIG. 1. (Color online) The neutron pattern (λ=1.594 Å) of $LiCrSi_2O_6$ sample collected at 15 K using the D2B diffractometer. The refinement has been done in the $P2_1/c$ space group with $a$=9.5121(5) Å, $b$=8.5728(4) Å, $c$=5.2241(3) Å and $\beta$ =109.7657(6)° with the following statistics (corrected from background): $R_p$=4.25% and $R_{wp}$=5.50%.

respectively. Neutron-diffraction measurements have also been recorded on $LiCrSi_2O_6$ samples in magnetic fields of up to 6 T at 2 K using a cryomagnet. The powder was pressed in tablets in order to preclude the grains' movement in the magnetic field. Diffraction data analysis was done using the FULLPROF refinement package.[14]

## III. RESULTS

### A. Crystal structure

The pattern was refined in the space group $P12_1/c1$, taking as starting structural model the structure reported by Redhammer and Roth.[9]

The refined lattice parameters are $a$=9.5355(3) Å, $b$ =8.5809(3) Å, $c$=5.24898(16) Å, and $\beta$=109.9303(5)° at room temperature. Within the error bars, our refinement at room temperature is similar to the single crystal reported previously.[9] Since the crystal structure of the pyroxene family has been investigated in details already in the literature, we shall present here only our results at 15 K. The good agreement between the calculated and observed patterns at 15 K is presented in Fig. 1.

The most characteristic parameters after the refinement are listed in Table I. A selection of the most important atomic distances and bonding angles are included in Tables II and III. Attempts of refinements of Cr and Li occupancies did not give evidence for the formation of vacancies neither for antisite disorder.

We recall here for the general reader the main structural features of the pyroxene family. This system exhibits a chain of edge-sharing $CrO_6$ octahedra running along the crystallographic axis $c$. These quasi-one-dimensional chains are connected by chains of $SiO_4$ tetrahedra. The packing of the $CrO_6$ octahedra chains linked by $SiO_4$ tetrahedra chains gives rise to a triangular magnetic lattice.

TABLE I. Crystallographic coordinates extracted from the Rietveld refinement carried out on powder neutron diffraction (D2B) using the space group $P12_1/c1$ at 15 K. The associated cell parameters are $a$=9.5121(5) Å, $b$=8.5728(4) Å, $c$=5.2241(3) Å, and $\beta$=109.7657(6)°.

| Atom | Wyckoff | $x$ | $y$ | $z$ |
|---|---|---|---|---|
| Li | 4$e$ | 0.2511(10) | 0.0109(7) | 0.2294(16) |
| Cr | 4$e$ | 0.2515(5) | 0.6582(4) | 0.2348(8) |
| $Si_1$ | 4$e$ | 0.0499(3) | 0.3412(4) | 0.2742(5) |
| $Si_2$ | 4$e$ | 0.5505(4) | 0.8409(4) | 0.2479(6) |
| $O_{1a}$ | 4$e$ | 0.8661(3) | 0.3327(3) | 0.1658(5) |
| $O_{1b}$ | 4$e$ | 0.3670(3) | 0.8348(3) | 0.1289(5) |
| $O_{2a}$ | 4$e$ | 0.1172(3) | 0.5118(3) | 0.3079(5) |
| $O_{2b}$ | 4$e$ | 0.6249(3) | 0.0059(3) | 0.3558(4) |
| $O_{3a}$ | 4$e$ | 0.1099(3) | 0.2696(3) | 0.5838(5) |
| $O_{3b}$ | 4$e$ | 0.6068(2) | 0.7180(3) | 0.5003(5) |

The $SiO_4$ tetrahedra form infinite chains running parallel to the $c$ axis and are interconnected by the $O_{3a}$ (or $O_{3b}$) oxygen atoms via shared corners. One chain is made of $Si_1$, $O_{1a}$, $O_{2a}$, and $O_{3a}$ while the other one is made of $Si_2$, $O_{1b}$, $O_{2b}$, and $O_{3b}$. They form two distinct chains in the $P2_1/c$ symmetry and one single chain in the high temperature form with the $C2/c$ symmetry. At 15 K, the S-rotated tetrahedra chains made from $Si_1$ are characterized by the angle $O_{3a}$-$O_{3a}$-$O_{3a}$= and the angle $O_{3b}$-$O_{3b}$-$O_{3b}$ for the O-rotated chains made from $Si_2$. The $O_{3a}$-$O_{3a}$-$O_{3a}$ angle is of 194.7(1)° and the $O_{3b}$-$O_{3b}$-$O_{3b}$ angle is of 156.3(1)° at 15 K.

Within the $CrO_6$ chains, there are two different magnetic interaction paths: Cr-$O_{1a}$-Cr and Cr-$O_{1b}$-Cr. The respective angles are 98.4(1)° and 97.8(1)° at room temperature. Within the error bars, these angles remain unchanged while lowering the temperature down to 1.8 K.

### B. Determination of the magnetic structure

The temperature dependence of the neutron powder-diffraction patterns collected as function of temperature on the D1B diffractometer is shown in Fig. 2. Below $T$ $\simeq$11.5 K, new diffraction peaks appear while some Bragg peaks increase in intensity. This confirms the appearance of a magnetic ordering below $T$=11.5 K, in good agreement with

TABLE II. Selected bond distances at room temperature in Å.

| $Cr^{3+}O_6$ | | $Si_1^{4+}O_4$ | | $Si_2^{4+}O_4$ | |
|---|---|---|---|---|---|
| Cr-$O_{1a}$ | 2.038(5) | $Si_1$-$O_{1a}$ | 1.647(4) | $Si_2$-$O_{1b}$ | 1.644(4) |
| Cr-$O_{1a}$ | 2.013(4) | $Si_1$-$O_{2a}$ | 1.582(4) | $Si_2$-$O_{2b}$ | 1.597(4) |
| Cr-$O_{1b}$ | 2.053(5) | $Si_1$-$O_{3a}$ | 1.641(4) | $Si_2$-$O_{3b}$ | 1.630(4) |
| Cr-$O_{1b}$ | 1.980(4) | $Si_1$-$O_{3a}$ | 1.613(4) | $Si_2$-$O_{3b}$ | 1.638(5) |
| Cr-$O_{2a}$ | 1.919(5) | | | | |
| Cr-$O_{2b}$ | 1.920(5) | | | | |

TABLE III. Selected bond angles at room temperature in degrees.

| | |
|---|---|
| Cr-$O_{1a}$-Cr | 97.7(2) |
| Cr-$O_{1b}$-Cr | 98.2(2) |
| $O_{1b}$-Cr-$O_{1a}$ | 176.0(2) |
| $O_{1b}$-Cr-$O_{1b}$ | 95.6(2) |
| $O_{1b}$-Cr-$O_{2a}$ | 89.2(2) |
| $O_{1b}$-Cr-$O_{2b}$ | 96.1(2) |

the magnetic data.[15] The magnetic reflections can be indexed by the propagation vector $\mathbf{k}=\mathbf{0}$.

The possible magnetic structures compatible with the symmetry of $LiCrSi_2O_6$ are determined by following the representation analysis technique described by Bertaut.[16] For the propagation vector $\mathbf{k}=\mathbf{0}$, the small group $G_{\mathbf{k}}$, formed by those elements of the space group that leave $\mathbf{k}$ invariant, coincides with the space group $P2_1/c$. For $\mathbf{k}=\mathbf{0}$, the irreducible representations of the group $G_{\mathbf{k}}$ are those shown in Table IV.[18]

A representation $\Gamma$ is constructed with the Fourier components $\mathbf{m}^{\mathbf{k}}$ corresponding to the Cr atoms of the Wyckoff position 4$e$. The Cr atoms at the site 4$e$ are denoted as (1) $(x,y,z)$, (2) $(\bar{x},y+\frac{1}{2},\bar{z}+\frac{1}{2})$, (3) $(\bar{x},\bar{y},\bar{z})$, and (4) $(x,\bar{y}+\frac{1}{2},z+\frac{1}{2})$. The decomposition of the representation $\Gamma$ in terms of the irreducible representations $\Gamma_{\mathbf{k}}$ is for the 4$e$ site,

$$\Gamma(4e) = 3\Gamma_1 + 3\Gamma_2 + 3\Gamma_3 + 3\Gamma_4. \quad (1)$$

We have four $Cr^{3+}$ ions per unit cell. Consequently, there are four different possible couplings between them: one ferromagnetic configuration and three antiferromagnetic ones. Equation (2) shows these four possibilities. The different basis vectors associated with each irreducible representation and calculated by using the projection operator technique implemented in BASIREPS.[17] They are presented in Table V. There are four possible magnetic structures. We have carried out refinements at the lowest measured temperature on D2B ($T$=1.8 K) with the four possible magnetic structures. We present in Fig. 3 the results of the refinements. The associated $R_{mag}$ factors associated to the models $\Gamma_j$ are 24.8%, 10.7%, 53.4%, and 7.7% for $\Gamma_1$, $\Gamma_2$, $\Gamma_3$, and $\Gamma_4$, respectively

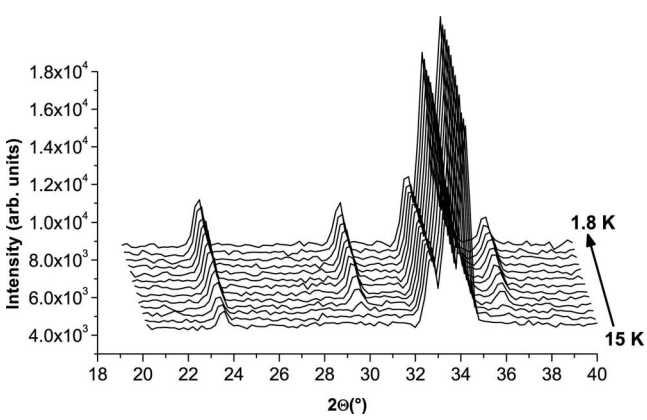


FIG. 2. Neutron diffraction patterns collected on the D1B diffractometer in the temperature range 1.8–15 K.

TABLE IV. Irreducible representations of the space group $P2_1/c$ for $\mathbf{k}=\mathbf{0}$. The symmetry elements are written according to Kovalev's notation (Ref. 18), $\tau=(0,\frac{1}{2},\frac{1}{2})$.

| | $h_1$ | $h_3/(\tau)$ | $h_{25}/(\tau)$ | $h_{27}/(\tau)$ |
|---|---|---|---|---|
| $\Gamma_1$ | 1 | 1 | 1 | 1 |
| $\Gamma_2$ | 1 | 1 | −1 | −1 |
| $\Gamma_3$ | 1 | −1 | 1 | −1 |
| $\Gamma_4$ | 1 | −1 | −1 | 1 |

$$\mathbf{M} = \mathbf{S}_1 + \mathbf{S}_2 + \mathbf{S}_3 + \mathbf{S}_4,$$

$$\mathbf{L}_1 = \mathbf{S}_1 - \mathbf{S}_2 + \mathbf{S}_3 - \mathbf{S}_4,$$

$$\mathbf{L}_2 = \mathbf{S}_1 + \mathbf{S}_2 - \mathbf{S}_3 - \mathbf{S}_4,$$

$$\mathbf{L}_3 = \mathbf{S}_1 - \mathbf{S}_2 - \mathbf{S}_3 + \mathbf{S}_4. \quad (2)$$

According to the experimental results the magnetic structure is given by the basis vectors of the irreducible representation $\Gamma_4$. This corresponds to a magnetic structure with the moments oriented mostly in the $ac$ plane with a small component along the $b$ axis, as shown in Fig. 4. The chains of $CrO_6$ octahedra are ferromagnetically coupled while the coupling within the chains is antiferromagnetic. The thermal evolution of the magnetic moments is displayed in Fig. 5. The magnetic components of the $Cr^{3+}$ ion determined using the D2B data at 1.8 K are $L_{2x}=2.12(4)\mu_B$; $L_{3y}=0.29(8)\mu_B$, and $L_{2z}=1.15(8)\mu_B$. The values of the magnetic moments reach saturation below 5 K and the orientation of the moments with respect to the $a$ axis remains nearly constant below $T_N$. The magnetic moment at $T$=1.8 K is $\|\mu(Cr^{3+})\| = 2.06(4)\mu_B$. This is about 16% of reduction compared to the saturation of the magnetic form factor of $Cr^{3+}$ determined experimentally which is $2.5\mu_B$.[19] This reduced magnetic moment could be interpreted as a result from the geometrical magnetic frustration presents in this system.

In Fig. 6, we show the temperature dependence of the cell parameters obtained from refinements of the D1B data. We observe no significant changes on passing through the Néel temperature. This observation suggests that the magnetostriction is extremely small in this material. This is confirmed by the refinements of the high-resolution data obtained at 1.8 and 15 K on the diffractometer D2B.

TABLE V. Basis vectors for the atoms of the 4$e$ site.

| Basis vectors | $x$ | $y$ | $z$ |
|---|---|---|---|
| $\Gamma_1$ | $L_{1x}$ | $M_y$ | $L_{1z}$ |
| $\Gamma_2$ | $L_{3x}$ | $L_{2y}$ | $L_{3z}$ |
| $\Gamma_3$ | $M_x$ | $L_{1y}$ | $M_z$ |
| $\Gamma_4$ | $L_{2x}$ | $L_{3y}$ | $L_{2z}$ |

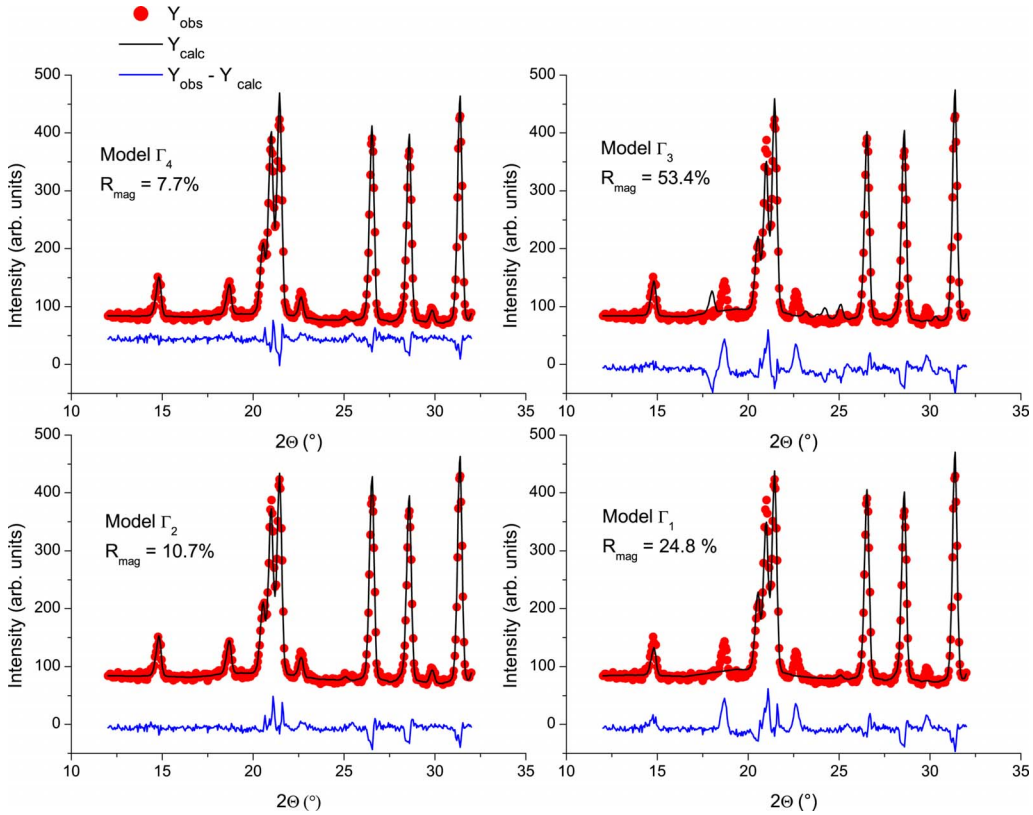


FIG. 3. (Color online) Fragment of the D2B neutron-diffraction pattern of $LiCrSi_2O_6$ at 1.8 K and refined by using the models with different orientation of the Cr magnetic moment.

### C. Study of the magnetic field dependence

In the work of Jodlauk *et al.*,[5] the authors claimed the existence of a structural phase transition induced by the magnetic field giving rise to a ferroelectric phase. Although these authors did not give any evidence for this statement (no hysteresis polarization loop was recorded), we have investigated the magnetic and crystal structures as function of magnetic field. We have measured $LiCrSi_2O_6$ at $T=2$ K on the diffractometer D2B under magnetic field using a cryomagnet up to 6 T. The powder was pressed in tablets in order to preclude the grains' movement in the magnetic field. We present a selected area of the recorded patterns where the changes as function of the magnetic field are the most important in Fig. 7.

The effect of the magnetic field is to reduce the magnetic moment from $2.06(4)\mu_B$ at zero field to $1.93(4)\mu_B$ at 6 T. This tendency is clearly confirmed by the progressive reduc-

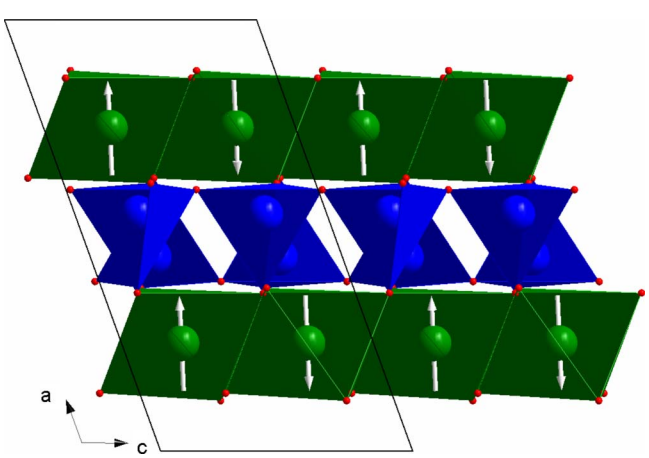


FIG. 4. (Color online) Magnetic structure of $LiCrSi_2O_6$. The magnetic coupling between the $CrO_6$ chains is ferromagnetic while the magnetic coupling within the chains is antiferromagnetic.

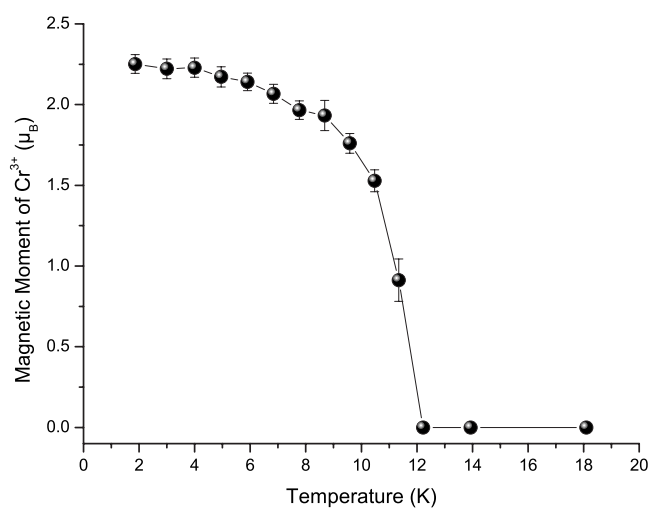


FIG. 5. Temperature dependence of the magnetic moment of $Cr^{3+}$ ions obtained from the refinement results of the D1B neutron diffractometer ($\lambda=2.52$ Å).

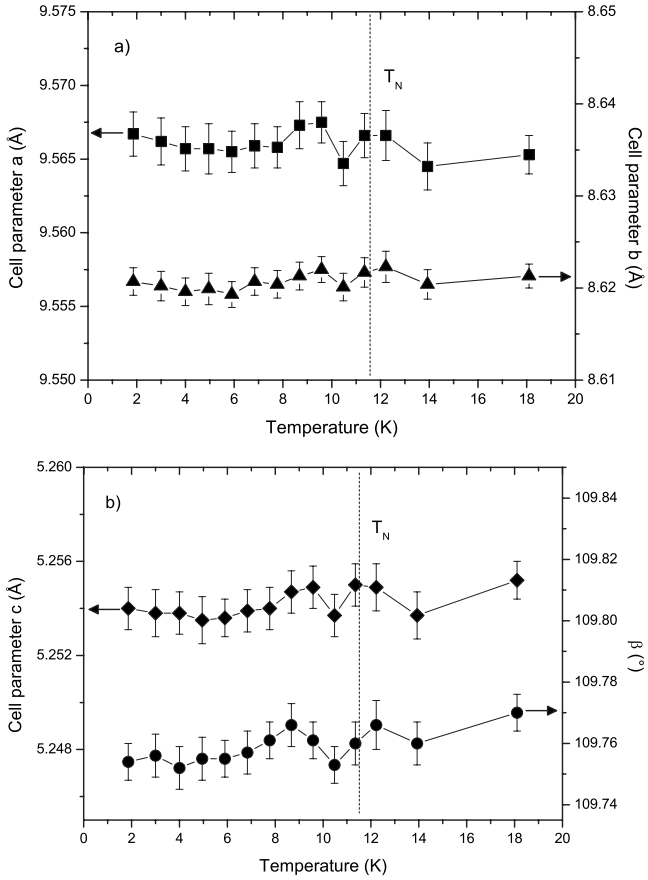


FIG. 6. Temperature dependence of the cell parameters as function of temperature in the range 1.8–18 K from the D1B data refinements (λ=2.52 Å). In (a), we show the cell parameters $a$ and $b$ and in (b) the cell parameter $c$ and the angle $\beta$.

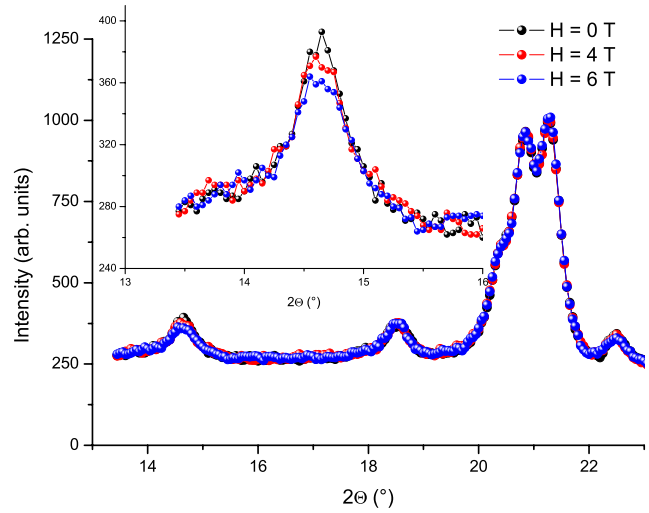


FIG. 7. (Color online) Neutron-diffraction patterns recorded at 2 K on pressed pellets of $LiCrSi_2O_6$ in magnetic field up to 6 T. In black, measurement was done with $H=0$ T, $H=4$ T, and $H=6$ T. The inset shows a zoom of the reflection (110) on which the variation of intensity is the most important.

tion in the magnetic intensity upon increasing magnetic field (see inset Fig. 7). Within the resolution of our data, we did not find any evidence for a magnetically induced ferroelectric phase. Our results suggest that $LiCrSi_2O_6$ is a linear magnetoelectric material in agreement with the magnetic structure at zero magnetic field.

## IV. PHENOMENOLOGICAL MODEL

In this section we describe a phenomenological model describing the magnetic ordering displayed by $LiCrSi_2O_6$ below its Néel temperature. In addition, we investigate the coupling terms giving rise to the linear magnetoelectric effect in this material.

We use here the notations for collinear structures described in Eq. (2) and the magnetic modes defined in Table V. The magnetic structure below $T_N$ is described by the irreducible representation $\Gamma_4$. This irreducible representation is characterized by the magnetic modes $L_{2x}$, $L_{3y}$, and $L_{2z}$. Experimentally, we have determined that the contribution $L_{3y}$ is smaller by a factor 4 to 7 compared to $L_{2x}$ or $L_{2z}$. Consequently in our phenomenological treatment, we will consider that only $\mathbf{L}_2$ has nonzero values below $T_N$. We can decompose the expression of the free energy $\Phi$ in several contributions: $\Phi=\Phi_0+\Phi_{ex}+\Phi_{rel}+\Phi_{me}+\Phi_H$.[20,21] The various coupling terms between the various order parameters are derived from symmetry considerations. Every product of the axial-vector components belonging to the same irreducible representation is invariant by time reversal and the crystal symmetry.[20] The minimization of the exchange part $\Phi_{ex}$ of the free energy determines only the relative orientation of the magnetic moments $\mathbf{S}_j$ with respect to each other

$$\Phi_{ex} = \frac{\zeta}{2}L_2^2 + \frac{\xi}{4}L_2^4 + \sum_i \frac{\chi_i}{2}M_i^2. \tag{3}$$

The variable $\zeta$ is the only parameter depending of the temperature such that $\zeta=\zeta_0(T-T_N)$. The $\frac{\chi_i}{2}$ terms are the components of the inverse magnetic susceptibility. The minimization of the relativistic part $\Phi_{rel}$ of the free energy will determine the orientation of the $\mathbf{S}_j$ with respect to the crystal axes[20]

$$\Phi_{rel} = \frac{1}{2}\sum_i \nu_i L_{2i}^2. \tag{4}$$

The reported magnetoelectric effect in $LiCrSi_2O_6$ requires the introduction in the thermodynamic potential of two additional contributions. One contribution must contain the possible magnetoelectric coupling terms which are of the type $L_iM_jP_k$. These terms are the couplings between the sublattice magnetization $L_i$, the total magnetization $M_j$, and the electrical polarization $P_k$. The other contribution is the magnetic energy[21]

$$\Phi_{me} = \lambda_1(L_{2x}+L_{2z})P_xM_y + \lambda_2(L_{2x}+L_{2z})P_zM_y + \lambda_3(L_{2x}+L_{2z})P_yM_x + \lambda_4(L_{2x}+L_{2z})P_yM_z + \sum_{i,j}\frac{\kappa_{i,j}}{2}P_j^2, \tag{5}$$

$$\Phi_H = -M \cdot H. \tag{6}$$

The $\lambda_i$ terms in $\Phi_{\mathrm{me}}$, which express the coupling of the order parameter (the antiferromagnetic order induced by $\mathbf{L}_2$) with the electrical polarization $\mathbf{P}$ and the magnetization $\mathbf{M}$, are of relativistic origin. The terms $\frac{\kappa_{i,j}}{2}$ are the tensor components of the inverse dielectric susceptibility. In $\Phi_{\mathrm{me}}$, we have also included quadratic terms in $\mathbf{P}$ which correspond to the dielectric energy. $\Phi_H$ will be taken into account for discussing the effect of the applied magnetic field.

Minimization of $\Phi$ with respect to the components of $\mathbf{P}$ and $\mathbf{M}$ yields the following relations:

$$P_x = -\frac{\lambda_1 L_x L_z M_y}{\kappa_x},$$

$$P_y = \frac{-\lambda_3 L_x L_z M_x - \lambda_4 L_x L_z M_z}{\kappa_y},$$

$$P_z = -\frac{\lambda_2 L_x L_z M_x}{\kappa_z}, \tag{7}$$

$$M_x = \frac{H_x - \lambda_3 L_x L_z P_y}{\chi_x},$$

$$M_y = \frac{H_y - \lambda_1 L_x L_z P_x - \lambda_2 L_x L_z P_z}{\chi_y},$$

$$M_z = \frac{H_z - \lambda_4 L_x L_z P_y}{\chi_z}. \tag{8}$$

As a consequence of relations given in Eqs. (7) and (8), one can work out the magnetic field induced polarization along the following three axes:

$$P_x = \frac{-\lambda_1 \kappa_z L_{2x} L_{2z}}{\chi_y \kappa_x \kappa_z - (\lambda_1^2 \kappa_z + \lambda_2^2 \kappa_x) L_{2x}^2 L_{2z}^2} H_y,$$

$$P_y = \frac{-\lambda_3 \chi_z L_{2x} L_{2z}}{\chi_x \chi_z \kappa_y - (\lambda_3^2 \chi_z + \lambda_4^2 \chi_x) L_{2x}^2 L_{2z}^2} H_x + \frac{-\lambda_4 \chi_x L_{2x} L_{2z}}{\chi_x \chi_z \kappa_y - (\lambda_3^2 \chi_z + \lambda_4^2 \chi_x) L_{2x}^2 L_{2z}^2} H_z,$$

$$P_z = \frac{-\lambda_2 \kappa_x L_{2x} L_{2z}}{\chi_y \kappa_x \kappa_z - (\lambda_1^2 \kappa_z + \lambda_2^2 \kappa_x) L_{2x}^2 L_{2z}^2} H_y. \tag{9}$$

Using the results of Eq. (9), we can write down the linear magnetoelectric tensor $P_i = \alpha_{ij} H_j$ corresponding to the irreducible representation $\Gamma_4$ (magnetic space group $P2_1'/c$),

$$\alpha_{\mathbf{ij}} = \begin{pmatrix} 0 & \alpha_{12} & 0 \\ \alpha_{21} & 0 & \alpha_{23} \\ 0 & \alpha_{32} & 0 \end{pmatrix}.$$

We note that this magnetoelectric tensor is in agreement with the linear magnetoelectric effect reported in $LiCrSi_2O_6$.[5] Indeed Jodlauk *et al.* reported an induced electrical polarization along the *b* axis while applying a magnetic field along the *c* axis. This corresponds to the linear magnetoelectric tensor term $\alpha_{23}$. This observation confirms that the magnetic structure that we have determined is in agreement with the reported linear magnetoelectric effect. Our phenomenological model is in agreement with the absence of field induced structural transition. The temperature dependence of $\alpha_{ij}$ can be modeled using Eq. (9). Knowing that $L^2$ is proportional to $\zeta$, we are able to find the temperature dependence of $\alpha_{ij}$. This is given in Fig. 8.

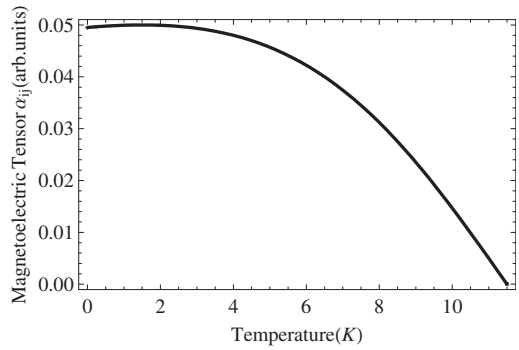


FIG. 8. Temperature dependence of the magnetoelectric coefficients $\alpha_{ij}$ given by Eq. (9) for $T_N = 11.5$ K.

Our phenomenological model also gives information about the two magnetic components of $\mathbf{L}_2$ becoming nonzero below $T_N$. If one assumes that $\lambda_i^2$ are small, one can work a simple expression for $L_{2x}$ and $L_{2z}$,

$$L_{2x}^2 = \frac{-\zeta(\xi + \gamma) + \gamma \nu_z + \xi \nu_x}{\xi^2 - \gamma^2},$$

$$L_{2z}^2 = \frac{-\zeta(\xi + \gamma) + \gamma \nu_x + \xi \nu_z}{\xi^2 - \gamma^2}, \tag{10}$$

where

$$\gamma = \left( \frac{H_y^2 \left( \frac{\lambda_1^2}{\kappa_x} + \frac{\lambda_2^2}{\kappa_z} \right)}{\chi_y^2} + \frac{(\chi_z H_x \lambda_3 + \chi_x H_z \lambda_4)^2}{\chi_x^2 \chi_z^2 \kappa_y} \right).$$

If there is no applied magnetic field, we find the usual expression for a magnetic component below its Néel temperature,[20]

$$L_{2x}^2 = \frac{-\zeta + \nu_x}{\xi},$$

$$L_{2z}^2 = \frac{-\zeta + \nu_z}{\xi}. \tag{11}$$

Looking at Eq. (11), one can notice that the relativistic contribution is important (terms in $\nu_x$ and $\nu_z$) in order to describe properly the magnetic order below $T_N$ ($L_{2x} \neq L_{2z}$).

## V. DISCUSSION

The crystal structure solution can be confirmed by calculation of the bond valence sum (BVS) for the various ions.[22]

The $Cr^{3+}$ ion is almost saturated (bond valence sum $[\Sigma s=2.95(2)]$ and the $Si^{4+}$ ions are also saturated $[\Sigma s=4.04(2)]$. The Li cation in pyroxenes generally is underbonded and possess valence sums of $\Sigma s=0.79-0.82$.[10] This is in agreement with our refinements at room temperature with $\Sigma s=0.801(8)$. It is assumed that the long Li-$O_3$ bond is responsible for the low valence sum (coordination number =5, Li-$O_{1a}$=2.071 Å; Li-$O_{1b}$=2.083 Å; Li-$O_{2a}$=2.183 Å; Li-$O_{2b}$=2.115 Å; Li-$O_{3a}$=2.318 Å).[10] The $O_{1a}$, $O_{1b}$, $O_{3a}$, and $O_{3b}$ oxygen atoms also are saturated in charge $[\Sigma s=2.046(13)$, 2.021(12), 2.077(13), and 1.990(13), respectively]. However, the $O_{2a}$ and $O_{2b}$ oxygen atoms possess a distinct deficit in negative charge [underbonded, $\Sigma s=1.849(12)$ and 1.851(13) respectively]. The apparent deficit in negative charge is compensated for by the short $Si_j$-$O_{2j}$ and Li-$O_{2j}$ bond lengths (see also Table II).

Neutron powder-diffraction experiments confirm that $LiCrSi_2O_6$ exhibits an antiferromagnetic ordering below $T_N=11.5$ K. The magnetic structure is commensurate with the chemical unit cell with $\mathbf{k}=\mathbf{0}$ with a magnetic moment of $Cr=2.06(4)\mu_B$. The magnetic space group displayed by $LiCrSi_2O_6$ is $P2_1'/c$ allowing a linear magnetoelectric effect in agreement with the reported induced electrical polarization along the $b$ axis when a magnetic field is applied along the $c$ axis.[5,23] Jodlauk *et al.*[15] suggested that this material exhibits a spiral magnetic structure resulting from the magnetic frustration. Our results show that this is not the case and that the magnetic frustration is small (magnetic moment reduced only by 16%) in agreement with the ratio $|\frac{\theta}{T_N}|=2.6$. This reduced magnetic moment is similar to what has been reported for $LiFeSi_2O_6$.[11] While magnetic frustration is obvious from considerations on the crystal structure of these pyroxenes, this family is not a good example of a spatially anisotropic triangular lattice[24] contrary to the expectations of Jodlauk *et al.*[5] This discrepancy can be explained by the fact that in the model proposed by Zhang *et al.*, there are only two antiferromagnetic coupling constants $J$ and not three like in $LiCrSi_2O_6$ as illustrated in Fig. 1 of Ref. 5. This probably explains the absence of spiral magnetic structure.

We notice also that our refinements suggest a magnetic symmetry which do not allow any ferromagnetic moment (no magnetic $M_j$ components belong to the irreducible representation $\Gamma_4$, see Table V). This is in perfect agreement with the reported magnetoelectric effect. However, this is in opposition with the reported small ferromagnetic moment of $0.005\mu_B$ by Jodlauk *et al.*[5] We believe that this moment is most likely the result of a small ferromagnetic impurity in their sample.

The linear magnetoelectric effect is strongly dependent on the magnetic symmetry of the system.[23] Jodlauk *et al.* have reported that they observe a magnetically induced electrical polarization not only in $LiCrSi_2O_6$ but also in $LiFeSi_2O_6$. Several studies using powder and single crystal report a magnetic structure described by the magnetic space group $P2_1/c$.[11,12] This magnetic symmetry forbids any linear magnetoelectric effect since it contains the inversion symmetry.[23] Consequently there is a discrepancy between the reported induced electrical polarization by Jodlauk *et al.* and the reported magnetic symmetry. Further investigations of the dielectric properties and reinvestigation of the magnetic structure of $LiFeSi_2O_6$ are necessary in order to resolve this discrepancy. Additionally, we notice that $LiVGe_2O_6$ has the same magnetic structure as $LiCrSi_2O_6$.[7] Consequently, the magnetic symmetry of $LiVGe_2O_6$ is compatible with the existence of a linear magnetoelectric effect.

## VI. CONCLUSION

We have investigated the magnetic and crystal structures of $LiCrSi_2O_6$ as function of temperature and magnetic field using powder neutron diffraction. Below $T_N=11.5$ K, $LiCrSi_2O_6$ exhibits a long-range antiferromagnetic order commensurate with the lattice with $\mathbf{k}=\mathbf{0}$. It is characterized by antiferromagnetic coupling within the $CrO_6$ chains and a ferromagnetic coupling between the chains. The associated magnetic symmetry is $P2_1'/c$ in agreement with the reported magnetoelectric effect. The magnetic field has for consequence to reduce the magnetic moment from 2.06(4) at zero field to $1.93(4)\mu_B$ at $H=6$ T. We propose a Landau phenomenological model describing the linear magnetoelectric effect in this material. We show that further investigations are required on the dielectric and magnetic properties of $LiFeSi_2O_6$ in order to understand the present discrepancies. Additionally, we notice that $LiVGe_2O_6$ has the same magnetic symmetry of $LiCrSi_2O_6$ and thus should exhibit a linear magnetoelectric effect.

## ACKNOWLEDGMENTS

We acknowledge Jacques Schweizer for critical reading of the manuscript. This study is partly supported by a Grant-in Aid for Scientific Research No. 19052008 and RFBR Grant No. 07-02-91201 from the Ministry of Education, Culture, Sports, Science and Technology of Japan and for JSPS (Japan)-RFBR (Russia) Joint Research Project.

*Corresponding author: Gwilherm Nénert. nenert@ill.eu. Present address: Institut Laue-Langevin, Boîte Postale 156, 6 rue Jules Horowitz, 38042 Grenoble Cedex 9, France.

[1] M. Fiebig, J. Phys. D **38**, R123 (2005).
[2] W. Eerenstein, N. D. Mathur, and J. F. Scott, Nature (London) **442**, 759 (2006).
[3] S.-W. Cheong and M. Mostovoy, Nat. Mater. **6**, 13 (2007).
[4] A. Pimenov, A. A. Mukhin, V. Yu. Ivanov, V. D. Travkin, A. M. Balbashov, and A. Loidl, Nat. Phys. **2**, 97 (2006); A. B. Sushkov, R. V. Aguilar, S. Park, S. W. Cheong, and H. D. Drew, Phys. Rev. Lett. **98**, 027202 (2007).
[5] S. Jodlauk, P. Becker, J. A. Mydosh, D. I. Khomskii, T. Lorenz, S. V. Streltsov, D. C. Hezel, and L. Bohatý, J. Phys.: Condens. Matter **19**, 432201 (2007).

[6] M. Isobe, E. Ninomiya, A. N. Vasiliev, and Y. Ueda, J. Phys. Soc. Jpn. **71**, 1423 (2002); S. V. Streltsov, O. A. Popova, and D. I. Khomskii, Phys. Rev. Lett. **96**, 249701 (2006).

[7] M. D. Lumsden, G. E. Granroth, D. Mandrus, S. E. Nagler, J. R. Thompson, J. P. Castellan, and B. D. Gaulin, Phys. Rev. B **62**, R9244 (2000).

[8] M. Isobe and Y. Ueda, J. Magn. Magn. Mater. **272-276**, 948 (2004); S. V. Streltsov and D. I. Khomskii, Phys. Rev. B **77**, 064405 (2008); G. J. Redhammer, H. Ohashi, and G. Roth, Acta Crystallogr., Sect. B: Struct. Sci. **59**, 730 (2003); C. Satto, P. Millet, and J. Galy, Acta Crystallogr., Sect. C: Cryst. Struct. Commun. **53**, 1727 (1997); P. Millet, F. Mila, F. C. Zhang, M. Mambrini, A. B. Van Oosten, V. A. Pashchenko, A. Sulpice, and A. Stepanov, Phys. Rev. Lett. **83**, 4176 (1999); E. Baum, W. Treutmann, M. Behruzi, W. Lottermoser, and G. Amthauer, Z. Kristallogr. **183**, 273 (1988); B. Pedrini, S. Wessel, J. L. Gavilano, H. R. Ott, S. M. Kazakov, and J. Karpinski, Eur. Phys. J. B **55**, 219 (2007); M. Isobe, Y. Ueda, A. N. Vasiliev, T. N. Voloshok, and O. L. Ignatchik, J. Magn. Magn. Mater. **258-259**, 125 (2003); A. N. Vasiliev, O. L. Ignatchik, A. N. Sokolov, Z. Hiroi, M. Isobe, and Y. Ueda, JETP Lett. **78**, 551 (2003).

[9] G. J. Redhammer, and G. Roth, Z. Kristallogr. **219**, 585 (2004). Please note that the coordinates given in the paper contain an error. The $x$ coordinate of $Si_1$ is 0.0487 and not 0.487.

[10] G. J. Redhammer and G. Roth, Z. Kristallogr. **219**, 278 (2004).

[11] G. J. Redhammer, G. Roth, W. Paulus, G. André, W. Lottermoser, G. Amthauer, W. Treutmann, and B. Koppelhuber-Bitschnau, Phys. Chem. Miner. **28**, 337 (2001).

[12] W. Lottermoser, G. J. Redhammer, K. Forcher, G. Amthauer, W. Paulus, G. André, and W. Treutmann, Z. Kristallogr. **213**, 101 (1998).

[13] O. Ballet, J. M. D. Coey, G. Fillion, A. Ghose, A. Hewat, and J. R. Regnard, Phys. Chem. Miner. **16**, 672 (1989).

[14] J. Rodriguez-Carvajal, Physica B **192**, 55 (1993).

[15] A. N. Vasiliev, O. L. Ignatchik, A. N. Sokolov, Z. Hiroi, M. Isobe, and Y. Ueda, Phys. Rev. B **72**, 012412 (2005).

[16] E. F. Bertaut, in *Magnetism*, edited by G. T. Rado and H. Shul (Academic, New York, 1963), Vol. III, Chap. 4.

[17] J. Rodríguez-Carvajal, BasIreps: A program for calculating irreducible representations of space groups and basis functions for axial and polar vector properties (see http://wwwold.ill.fr/dif/Soft/fp/php/downloads.html).

[18] O. V. Kovalev, in *Representations of the Crystallographic Space Groups: Irreducible Representations, Induced Representations and Corepresentations*, edited by H. T. Stokes and D. M. Hatch (Gordon and Breach, Amsterdam, 1993).

[19] P. J. Brown, J. B. Forsyth, and F. Tasset, Solid State Sci. **7**, 682 (2005).

[20] J.-C. Tolédano and P. Tolédano, *The Landau Theory of Phase Transitions* (World Scientific, Singapore, 1987).

[21] P. Toledano, Ferroelectrics **161**, 257 (1994).

[22] N. E. Brese and M. O'Keefee, Acta Crystallogr. B **47**, 192 (1991); I. D. Brown, *ibid.* **48**, 553 (1992).

[23] *International Tables for Crystallography in Physical Properties of Crystals*, edited by A. Authier (Kluwer, Dordrecht, 2003), Vol. D.

[24] W. M. Zhang, W. M. Saslow, and M. Gabay, Phys. Rev. B **44**, 5129 (1991).